

# The SOX experiment: understanding the detector behavior using calibration sources

A. Caminata<sup>1</sup>, M. Agostini<sup>2</sup>, K. Altenmüller<sup>2</sup>, S. Appel<sup>2</sup>, G. Bellini<sup>3</sup>, J. Benziger<sup>4</sup>, N. Berton<sup>5</sup>, D. Bick<sup>6</sup>, G. Bonfini<sup>7</sup>, D. Bravo<sup>8</sup>, B. Caccianiga<sup>3</sup>, F. Calaprice<sup>9</sup>, M. Carlini<sup>7</sup>, P. Cavalcante<sup>7</sup>, A. Chepurinov<sup>10</sup>, K. Choi<sup>11</sup>, M. Cribier<sup>5</sup>, D. D'Angelo<sup>3</sup>, S. Davini<sup>12</sup>, A. Derbin<sup>13</sup>, L. Di Noto<sup>1</sup>, I. Drachnev<sup>12</sup>, M. Durer<sup>5</sup>, A. Etenko<sup>14</sup>, S. Farinon<sup>1</sup>, V. Fischer<sup>5</sup>, K. Fomenko<sup>15</sup>, A. Formozov<sup>3,15</sup>, D. Franco<sup>16</sup>, F. Gabriele<sup>7</sup>, J. Gaffiot<sup>5</sup>, C. Galbiati<sup>9</sup>, C. Ghiano<sup>1</sup>, M. Giammarchi<sup>3</sup>, M. Goeger-Neff<sup>2</sup>, A. Goretti<sup>9</sup>, M. Gromov<sup>10</sup>, C. Hagner<sup>6</sup>, Th. Houdy<sup>5</sup>, E. Hungerford<sup>17</sup>, Aldo Ianni<sup>7</sup>, Andrea Ianni<sup>9</sup>, N. Jonquères<sup>18</sup>, K. Jedrzejczak<sup>19</sup>, D. Jeschke<sup>2</sup>, M. Kaiser<sup>6</sup>, V. Kobychew<sup>20</sup>, D. Korablev<sup>15</sup>, G. Korga<sup>7</sup>, V. Kornoukhov<sup>21</sup>, D. Kryn<sup>16</sup>, T. Lachenmaier<sup>22</sup>, T. Lasserre<sup>5</sup>, M. Laubenstein<sup>7</sup>, B. Lehnert<sup>23</sup>, J. Link<sup>8</sup>, E. Litvinovich<sup>14,24</sup>, F. Lombardi<sup>7</sup>, P. Lombardi<sup>3</sup>, L. Ludhova<sup>3</sup>, G. Lukyanchenko<sup>14,24</sup>, I. Machulin<sup>14,24</sup>, S. Manecki<sup>8</sup>, W. Maneschg<sup>28</sup>, S. Marcocci<sup>12</sup>, J. Maricic<sup>11</sup>, G. Mention<sup>5</sup>, E. Meroni<sup>3</sup>, M. Meyer<sup>6</sup>, L. Miramonti<sup>3</sup>, M. Misiaszek<sup>7,19</sup>, M. Montuschi<sup>25</sup>, P. Mosteiro<sup>9</sup>, V. Muratova<sup>13</sup>, R. Musenich<sup>1</sup>, B. Neumair<sup>2</sup>, L. Oberauer<sup>2</sup>, M. Obolensky<sup>16</sup>, F. Ortica<sup>26</sup>, M. Pallavicini<sup>1</sup>, L. Papp<sup>2</sup>, L. Perasso<sup>1</sup>, A. Pocar<sup>27</sup>, G. Ranucci<sup>3</sup>, A. Razeto<sup>7</sup>, A. Re<sup>3</sup>, A. Romani<sup>26</sup>, R. Roncin<sup>7,16</sup>, N. Rossi<sup>7</sup>, S. Schönert<sup>2</sup>, L. Scola<sup>5</sup>, D. Semenov<sup>13</sup>, H. Simgen<sup>28</sup>, M. Skorokhvatov<sup>14,24</sup>, O. Smirnov<sup>15</sup>, A. Sotnikov<sup>15</sup>, S. Sukhotin<sup>13</sup>, Y. Suvorov<sup>14,29</sup>, R. Tartaglia<sup>7</sup>, G. Testera<sup>1</sup>, J. Thurn<sup>23</sup>, M. Toropova<sup>14</sup>, C. Veyssiére<sup>5</sup>, M. Vivier<sup>5</sup>, E. Unzhakov<sup>13</sup>, R.B. Vogelaar<sup>8</sup>, F. von Feilitzsch<sup>2</sup>, H. Wang<sup>29</sup>, S. Weinz<sup>30</sup>, J. Winter<sup>30</sup>, M. Wojcik<sup>19</sup>, M. Wurm<sup>30</sup>, Z. Yokley<sup>8</sup>, O. Zaimidoroga<sup>15</sup>, S. Zavatarelli<sup>1</sup>, K. Zuber<sup>23</sup>, G. Zuzel<sup>19</sup>

<sup>1</sup>Dipartimento di Fisica, Università degli Studi e INFN, Genova 16146, Italy

<sup>2</sup>Physik-Department and Excellence Cluster Universe, Technische Universität München, 85748 Garching, Germany

<sup>3</sup>Dipartimento di Fisica, Università degli Studi e INFN, 20133 Milano, Italy

<sup>4</sup>Chemical Engineering Department, Princeton University, Princeton, NJ 08544, USA

<sup>5</sup>Commissariat à l'Énergie Atomique et aux Énergies Alternatives, Centre de Saclay, IRFU, 91191 Gif-sur-Yvette, France

<sup>6</sup>Institut für Experimentalphysik, Universität Hamburg, 22761 Hamburg, Germany

<sup>7</sup>INFN Laboratori Nazionali del Gran Sasso, 67010 Assergi (AQ), Italy

<sup>8</sup>Physics Department, Virginia Polytechnic Institute and State University, Blacksburg, VA 24061, USA

<sup>9</sup>Physics Department, Princeton University, Princeton, NJ 08544, USA

<sup>10</sup>Lomonosov Moscow State University Skobeltsyn Institute of Nuclear Physics, 119234 Moscow, Russia

<sup>11</sup>Department of Physics and Astronomy, University of Hawai'i, Honolulu, HI 96822, USA

<sup>12</sup>Gran Sasso Science Institute (INFN), 67100 L'Aquila, Italy

<sup>13</sup>St. Petersburg Nuclear Physics Institute NRC Kurchatov Institute, 188350 Gatchina, Russia

<sup>14</sup>NRC Kurchatov Institute, 123182 Moscow, Russia

<sup>15</sup>Joint Institute for Nuclear Research, 141980 Dubna, Russia

<sup>16</sup>AstroParticule et Cosmologie, Universit Paris Diderot, CNRS/IN2P3, CEA/IRFU, Observatoire de Paris, Sorbonne Paris Cit, 75205 Paris Cedex 13, France

<sup>17</sup>Department of Physics, University of Houston, Houston, TX 77204, USA

<sup>18</sup>Commissariat à l'Énergie Atomique et aux Énergies Alternatives, Centre de Saclay, DEN/DM2S/SEMT/BCCR, 91191 Gif-sur-Yvette, France

<sup>19</sup>M. Smoluchowski Institute of Physics, Jagiellonian University, 30059 Krakow, Poland

<sup>20</sup>Kiev Institute for Nuclear Research, 06380 Kiev, Ukraine

<sup>21</sup>Institute for Theoretical and Experimental Physics, 117218 Moscow, Russia

<sup>22</sup>Kepler Center for Astro and Particle Physics, Universität Tübingen, 72076 Tübingen, Germany

<sup>23</sup>Department of Physics, Technische Universität Dresden, 01062 Dresden, Germany

<sup>24</sup>National Research Nuclear University MEPhI (Moscow Engineering Physics Institute), 115409 Moscow, Russia

<sup>25</sup>Dipartimento di Fisica e Scienze della Terra Università degli Studi di Ferrara e INFN, Via Saragat 1-44122, Ferrara, Italy

<sup>26</sup>Dipartimento di Chimica, Università e INFN, 06123 Perugia, Italy

<sup>27</sup>Amherst Center for Fundamental Interactions and Physics Department, University of Massachusetts, Amherst, MA 01003, USA

<sup>28</sup>Max-Planck-Institut für Kernphysik, 69117 Heidelberg, Germany

<sup>29</sup>Physics and Astronomy Department, University of California Los Angeles (UCLA), Los Angeles, California 90095, USA

<sup>30</sup>Institute of Physics and Excellence Cluster PRISMA, Johannes Gutenberg-Universität Mainz, 55099 Mainz, Germany

**DOI:** <http://dx.doi.org/10.3204/DESY-PROC-2016-05/22>

The SOX experiment investigates the existence of light sterile neutrinos. A solid signal would mean the discovery of the first particles beyond the Standard Electroweak Model and would have profound implications in our understanding of the Universe and of fundamental particle physics. In case of a negative result, it is able to close a long standing debate about the reality of the neutrino anomalies. The SOX experiment will use a  $^{144}\text{Ce} - ^{144}\text{Pr}$  antineutrino generator placed 8.5 m below the Borexino liquid scintillator detector. In view of the SOX experiment, a precise knowledge of the energy response and the spatial reconstruction of the antineutrino events is very important. Consequently, a calibration campaign of the Borexino detector is foreseen before the beginning of the SOX data taking. This paper briefly reviews the techniques used for calibrate the Borexino detector.

## 1 Introduction

Although most of the collected neutrino experimental data are explainable within the three-flavor oscillation model, some short-baseline neutrino experiment have reported results that significantly deviates from the three active neutrino picture ([1, 2, 3, 4]), suggesting a possible short distance oscillation between the three known neutrino states and one hypothetical new state with a squared mass  $\Delta m_{14}^2$  of about  $1 \text{ eV}^2$ . Due to constraints on Z boson coupling asserted by LEP, this state would be sterile.

The SOX project aims to test the existence of light sterile neutrinos detecting the antineu-

trino flux coming from a 150 kCi  $^{144}\text{Ce} - ^{144}\text{Pr}$  source placed at short distance from the Borexino liquid scintillator detector [5] (figure 1). Antineutrinos are detected inside Borexino via inverse beta decay, thus with a negligible background [6]. Borexino will investigate short distance neutrino oscillations in two ways. The first way is the standard disappearance technique (rate technique). Knowing the source activity and measuring the interaction rate, it is possible to investigate the existence of the sterile neutrino state. The second way is based on an oscillometry measurement within the detector volume (shape technique). Expected sensitivities are shown in figure 2.

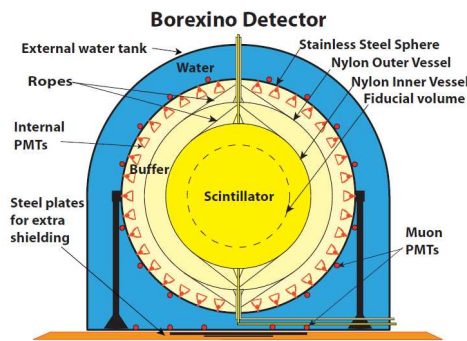


Figure 1: Schematic drawing of the Borexino detector.

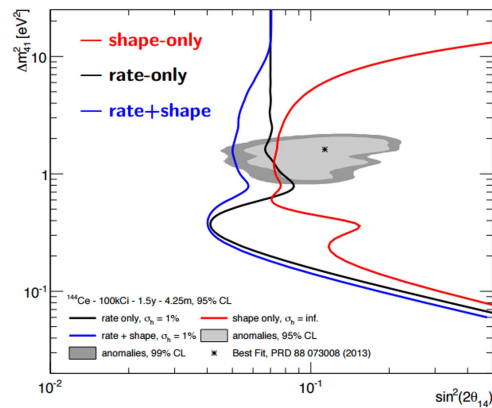


Figure 2: Neutrino anomaly region and foreseen sensitivity for SOX.

## 2 Motivation for a calibration campaign and Borexino source insertion system

A good knowledge of the Borexino detector response is a key requirement for the SOX analysis. Given the large dimensions of the detector, it is necessary to map the energy response and the position reconstruction accuracy in the whole active volume. Since the energy of the incoming antineutrino is reconstructed from the positron energy, the knowledge of the energy scale is mandatory. Consequently, a Monte Carlo simulation code have been developed and the detector response have been tested deploying radioactive sources in several positions (2008 and 2009 calibration campaigns [7]). These data are extremely useful in view of the SOX experiment. Since the SOX and geoneutrino signals have the same features, calibration data acquired for the geoneutrino analysis can be used also for SOX. Nevertheless, a new calibration campaign is foreseen before the arrival of the SOX antineutrino source. These calibration data are of extreme importance in understanding the detector behavior and to increase the reliability of the SOX Monte Carlo simulation code. Since in the SOX analysis the cut efficiencies and the sensitivity studies are performed analyzing the output of the simulations, having an accurate simulation code is crucial for a proper data analysis.

Sources are inserted in Borexino by means of a series of hollow interconnecting rods in a 4'' pipe connecting the top of the detector with the liquid scintillator (figure 1). One special rod has

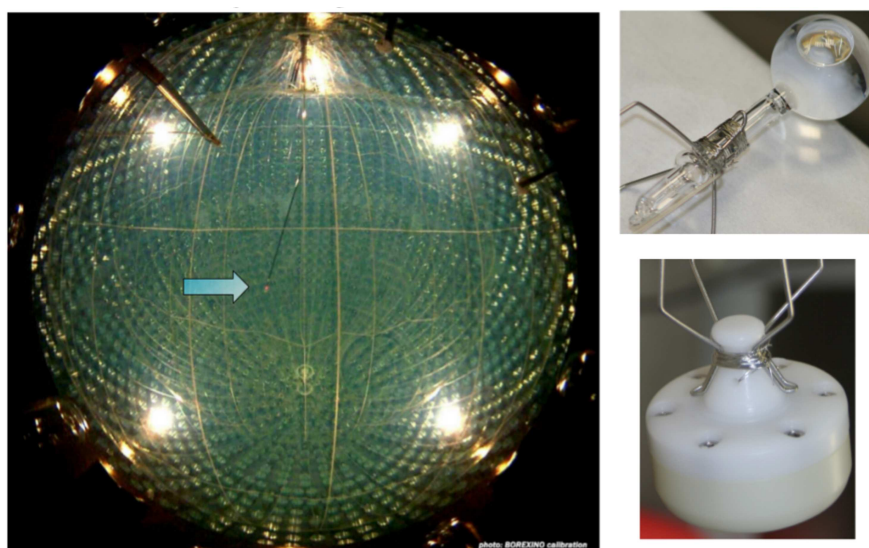


Figure 3: Left: picture shot by a CCD camera. The insertion system is visible and it is pointed by the blue arrow. Right: vials used for gamma (top) and neutron (bottom) sources.

an hinge that allows the arm to bend up to  $90^\circ$  and thus reaching most of the detector's active zone. Since it is important to know the position of the inserted source, a source location system have been developed. The system has to find the exact coordinate of the position in which the source is deployed. This information is crucial for estimating the position reconstruction accuracy. Consequently, seven CCD cameras look for the position of a red (wavelength about 630 nm) light diffuser attached close to the source (figure 3). The system is able to locate the source within 1 cm. The wavelength of this light has been chosen so as not to be harmful to the PMTs under HV.

### 3 Calibration campaign

#### 3.1 Past calibration campaign

Gamma radioactive sources were dissolved in aqueous solution and contained in small quartz vials.  $\alpha$  and  $\beta$  radioactive sources ( $^{14}\text{C}$  –  $^{222}\text{Rn}$ ) were contained in a quartz vial as well but scintillator was used as solvent. Table 1 shows all the sources used for calibration purpose.

A deep understanding of the detector response to the gamma sources is fundamental for the SOX analysis since the energy deposit of the prompt event is due to both positron interaction with matter and to positron-electron annihilation.

The  $^{241}\text{Am}$  –  $^9\text{Be}$  neutron source calibration was performed mainly for solar neutrino ( $^8\text{B}$ ) and geoneutrino analyses. Nevertheless, they are of fundamental importance for SOX, since the delayed event is due to neutron capture. In the  $^{241}\text{Am}$  –  $^9\text{Be}$  neutron source, neutrons are produced in association with gammas, with a total energy releas of 4.44 MeV. Similarly to the SOX signal, the  $^{241}\text{Am}$  –  $^9\text{Be}$  source provides a prompt and a delayed event (figure 4). The prompt event is due to the gamma energy loss together with the signal of proton recoils

Source	Type	E [MeV]	Position	Motivations	Campaign
$^{57}\text{Co}$	$\gamma$	0.122	in IV volume	Energy scale	IV
$^{139}\text{Ce}$	$\gamma$	0.165	in IV volume	Energy scale	IV
$^{203}\text{Hg}$	$\gamma$	0.279	in IV volume	Energy scale	III
$^{85}\text{Sr}$	$\gamma$	0.514	z-axis + sphere R=3 m	Energy scale + FV	III,IV
$^{54}\text{Mn}$	$\gamma$	0.834	along z-axis	Energy scale	III
$^{65}\text{Zn}$	$\gamma$	1.115	along z-axis	Energy scale	III
$^{60}\text{Co}$	$\gamma$	1.173, 1.332	along z-axis	Energy scale	III
$^{40}\text{K}$	$\gamma$	1.460	along z-axis	Energy scale	III
$^{222}\text{Rn} + ^{14}\text{C}$	$\beta, \gamma$	0-3.20	in IV volume	FV+uniformity	I-IV
	$\alpha$	5.5, 6.0, 7.4	in IV volume	FV+uniformity	
$^{241}\text{Am} + ^9\text{Be}$	n	0-9	sphere R=4 m	Energy scale + FV	II-IV
394 nm laser	light	-	center	PMT equalization	IV

Table 1: Radioactive sources used during the Borexino internal calibration campaigns. The radionuclides, energies and emitted particle types are shown in the first three columns. The fourth column indicates the positions where the sources were deployed within the scintillator. The main purposes for the individual source measurements are summarized in the fifth column. The last column indicates in which campaign the sources have been deployed: I (October 2008), II (January 2009), III (June 2009) and IV (Jul 2009). FV is the fiducial volume used in the solar analysis [8], the corresponding sources were used to evaluate the event position reconstruction performances.

due to interaction of neutron with the scintillator. Afterwards, neutrons thermalize in the hydrogen-rich organic scintillator and are captured either on protons or carbon nuclei, emitting characteristic 2.22 MeV and 4.95 MeV  $\gamma$  rays (figure 4). These  $\gamma$  rays produce a delayed signal according to the neutron capture time of about 254  $\mu\text{s}$ .

### 3.2 Next calibration campaign

Next calibration campaign will take place next fall just before the SOX source arrival. During next calibration campaign both gamma and AmBe sources will be deployed inside Borexino. This calibration will be very useful both for phase 2 solar neutrino analysis (precision measurement of solar neutrino fluxes) and for SOX. Differently from old calibration campaigns, there will be an extensive calibration with AmBe source, especially nearby the inner vessel. The calibration points at large radii will be extremely important to study the neutron detection efficiency at the border of the active zones.

## 4 Conclusions

The SOX experiment aims to investigate the existence of sterile neutrinos placing a high activity  $^{144}\text{Ce} - ^{144}\text{Pr}$  antineutrino source below the Borexino detector. Both a rate analysis and a shape analysis are foreseen. For both the analyses, a deep understanding of the detector response is necessary. In the past years, the detector have been calibrated deploying several sources in the active volume. A new calibration campaign is foreseen for the end of this year, just before the beginning of SOX data-taking.

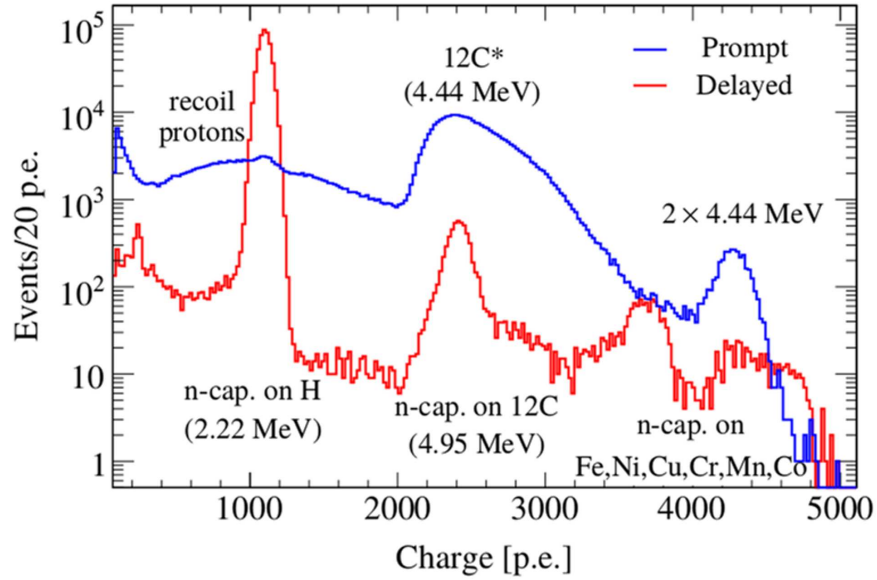


Figure 4: Energy spectrum of the  $^{241}\text{Am}-^9\text{Be}$  source. The spectrum is subdivided in neutron-induced prompt signal (blue) and delayed signals (red).

## References

- [1] Aguilar A *et al.* 2001 *Phys. Rev. D* **64** 112007
- [2] Aguilar A *et al.* 2013 *Phys. Rev. Lett.* **110** 161801
- [3] Mention G *et al.* 2011 *Phys. Rev. D* **83** 073006
- [4] Giunti C and Laveder M 2011 *Phys. Rev. C* **83** 065504
- [5] Bellini G *et al.* 2013 *JHEP* **38** 1308
- [6] Agostini M *et al.* 2015 *Phys. Rev. D* **92** 031101
- [7] Bellini G *et al.* 2012 *Journal of Instrumentation* **7** 10018
- [8] Bellini G *et al.* 2014 *Phys. Rev. D* **89** 112007